Far-Field Analysis of Coupled Bulk and Boundary Layer Diffusion Toward an Ion Channel Entrance

Mark F. Schumaker and C. J. Kentler
Department of Pure and Applied Mathematics, Washington State University, Pullman, Washington 99164-3113 USA

ABSTRACT We present a far-field analysis of ion diffusion toward a channel embedded in a membrane with a fixed charge density. The Smoluchowski equation, which represents the 3D problem, is approximated by a system of coupled three- and two-dimensional diffusions. The 2D diffusion models the quasi-two-dimensional diffusion of ions in a boundary layer in which the electrical potential interaction with the membrane surface charge is important. The 3D diffusion models ion transport in the bulk region outside the boundary layer. Analytical expressions for concentration and flux are developed that are accurate far from the channel entrance. These provide boundary conditions for a numerical solution of the problem. Our results are used to calculate far-field ion flows corresponding to experiments of Bell and Miller (*Biophys. J.* 45:279, 1984).

GLOSSARY

Symbols that appear in two or more sections of the text are listed. When uppercase and lowercase symbols are given together, lowercase denotes dimensionless quantities. We follow a common convention and do not distinguish by symbol between functions representing the same physical quantity on the same physical domain but represented in different coordinate systems.

Latin symbols

a	Radius of channel entrance
b	Far-field capture radius
C_b, c_b	Bulk concentration in Boundary Surface Model
C_p, c_p	Concentration of permeant ion in Boundary Layer Model
C_s, c_s	Surface concentration in Boundary Surface Model
C_s^∞, c_s^∞	Surface concentration far from channel entrance
C_0	Bulk concentration far from channel entrance
D	Permeant ion diffusion coefficient
e_0	Elementary electrical charge
F_b, F_s, F_T	Bulk, surface, and total ion flux toward channel entrance
h	Lattice spacing
J_b, J_s	Bulk and surface flux densities
K_{bs}, k_{bs}	Rate constant from bulk to surface
K_{sb}, k_{sb}	Rate constant from surface to bulk
K_{se}	Rate constant for ion entrance into channel
k_B	Boltzmann's constant
n	Number of lattice sites along one spatial coordinate in random walk or numerical solution
r	Radial variable in Boundary Layer spherical coordinates
s	Radial variable in Boundary Surface spherical coordinates
T	Absolute temperature
$\bar{T}$	Mean time before leaving boundary surface
$\hat{T}$	Mean time before leaving physical surface layer
t, t_0, Δt	Time, a fixed time, time step
X, x, Y, y	Cartesian coordinates in the plane of the membrane
Z, z	Spatial coordinate normal to membrane surface

Greek symbols

ϵ	Spacing between 0 and ϵ rows as a fraction of h
ζ	Coordinate normal to membrane in physical surface layer
ζ_0	depth of boundary layer
θ	Polar angle in spherical polar coordinates
κ	The membrane association constant K_{bs}/K_{sb}
ρ, $\hat{\rho}$	Radial variable in cylindrical coordinates, dimensionless radial variable
$\Delta\tau$	A fixed time step, independent of n
Ψ, ψ	Macroscopic electrical potential of permeant ion

INTRODUCTION

Understanding the role of surface diffusion is a problem of widespread interest in biophysics, as in the area of chemoreception, for example (Adams and Delbrück, 1968; Berg

Received for publication 27 May 1997 and in final form 6 February 1998.
Address reprint requests to Dr. Mark F. Schumaker, Department of Pure and Applied Mathematics, Washington State University, Pullman, WA 99164-3113. Tel.: 509-335-3170; Fax: 509-335-1188; E-mail: schumaker@wsn.edu.

0006-3495/98/05/2235/14 $2.00

and Purcell, 1977). There is experimental evidence that a similar mechanism can also play a very important role in ion transport from solution to an ion channel entrance. Negatively charged lipid bilayers greatly enhance cation channel conductance, especially at low ionic strength (Apell et al., 1979; Bell and Miller, 1984; Aguilella et al., 1997). A straightforward interpretation is that cations are attracted to a concentrated surface layer close to the membrane surface, where they undergo a quasi-two-dimensional diffusion, and then enter the channel from the concentrated layer. We shall call this quasi-two-dimensional transport mechanism *boundary layer diffusion*.

As information regarding the three-dimensional structure of membrane channels becomes available, it will be desirable to build detailed spatial models of ion conduction toward membrane channels. These would offer further insight into the role of boundary layer diffusion. One approach would be to solve the Smoluchowski equation with appropriate boundary data:

$$D\nabla^2 C_p + D\nabla \cdot (\nabla\psi\, C_p) = 0, \tag{1}$$

where C_p is the permeant ion concentration, D is a diffusion coefficient, and $\psi = e_0\Psi/k_BT$ is the dimensionless electrical potential. Physically, the Smoluchowski equation models ion movement as being due to diffusion under the influence of the electrical field $-\nabla\Psi$ (e.g., Risken, 1989). Concentrations are assumed to be time independent.

This paper presents a far-field analysis of boundary layer diffusion for a simplified system that approximates Eq. 1. A partial solution is obtained that incorporates only the boundary conditions far from the channel entrance. In this region, the flow field does not depend on the details near the entrance, but only on properties of the solution and membrane. The far-field analysis offers direct insight into the role of boundary layer diffusion and yields boundary conditions in solution a finite distance from the channel that are used for a numerical solution.

We now consider two models of an ion channel in a membrane, introduce terminology, and state simplifying assumptions. The Boundary Layer Model solves Eq. 1 for a single channel in a planar membrane, as sketched in Fig. 1 *A*. The coordinate ζ is perpendicular to the plane of the membrane. Ions in solution screen a fixed membrane charge density, and the resultant electrical potential decays rapidly as ζ increases. We choose ζ_0 so that the potential is significant only in the boundary layer region, $0 < \zeta < \zeta_0$. The ion channel entrance structure is also contained in the boundary layer, and may be described by very complicated boundary conditions. The bulk region corresponds to $\zeta > \zeta_0$. Here the electric field associated with the membrane charge density is weak, and the second term in Eq. 1 is unimportant.

The Boundary Surface Model of Fig. 1 *B* simplifies this geometry, allowing a useful mathematical analysis. The coordinate $Z = \zeta - \zeta_0$, $Z > 0$ models the bulk region above the boundary layer. In this region, the ion concentration is

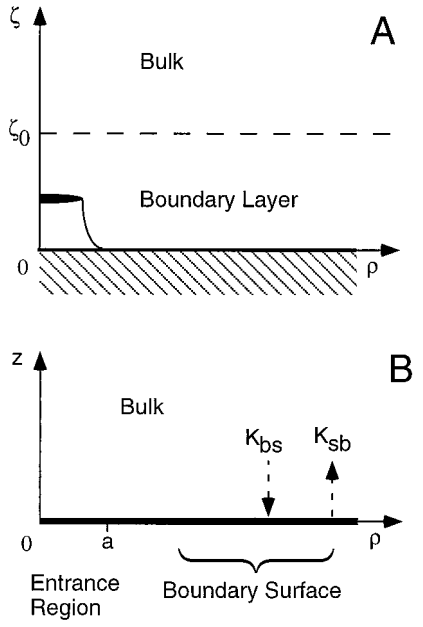

FIGURE 1 (*A*) Boundary Layer Model of ion diffusion in the vicinity of an ion channel entrance. An attractive interaction between the ions and membrane surface is mostly confined to a boundary layer of thickness ζ_0. ρ and ζ are cylindrical coordinates. An ion channel entrance may be associated with complex boundary conditions near the origin. (*B*) Boundary Surface Model for far-field analysis. Transport within the boundary layer is represented by diffusion on a two-dimensional boundary surface. Ions in the bulk are assumed to diffuse free of any interaction with the surface. Ion movements between the bulk and surface are modeled by rate constants K_{bs} and K_{sb}, as described in the text. The channel is represented by an entrance region on the boundary surface, where ion absorption is described by another rate constant.

described as a solution of Laplace's equation:

$$\nabla^2 C_b(\rho, Z) = 0, \tag{2}$$

where C_b is the ion concentration and (ρ, Z) are cylindrical coordinates, assuming azimuthal symmetry. Next we integrate the boundary layer over the interval $0 < \zeta < \zeta_0$, reducing it to a 2D boundary surface. Rate constants K_{bs} and K_{sb} are introduced and adjusted to model the unidirectional fluxes of ions between the boundary surface and the bulk, far from the ion channel entrance. The expression for the net flux density out of the boundary surface is

$$-D\frac{\partial C_b}{\partial Z}(\rho, 0) = C_s(\rho)K_{sb} - C_b(\rho, 0)K_{bs}. \tag{3}$$

where $C_s(\rho)$ is the concentration on the boundary surface. Diffusion in the boundary surface itself is modeled by a 2D Poisson's equation, where the right-hand side corresponds to the flux density out of the surface:

$$D\nabla^2 C_s(\rho) = C_s(\rho)K_{sb} - C_b(\rho, 0)K_{bs}. \tag{4}$$

Equations 2–4 describe the Boundary Surface Model used for the far-field analysis. In the Methods section we first derive them as the diffusion limit of a random walk, showing that they do consistently represent coupled 2D and

3D diffusions. We next show how K_{bs} and K_{sb} can be chosen to model average properties of transport to and from the boundary layer. A multipole expansion of Laplace's equation is then used to obtain an asymptotic expression for the solution of the Boundary Surface equations valid in the far field. The asymptotic expressions are used to obtain boundary conditions suitable for a numerical study.

A result of our analysis is that the solution in the far field only depends on the details at the channel entrance through the total current flowing into the channel. Our numerical solution has a simple representation of the channel entrance, which allows the total current to be adjusted. In the entrance region, $\rho < a$ of Fig. 1 *B*, an additional rate constant K_{se} is introduced on the right-hand side of Poisson's equation:

$$D\nabla^2 C_s(\rho) = C_s(\rho)(K_{sb} + K_{se}) - C_b(\rho, 0)K_{bs}. \quad (5)$$

K_{se} is adjusted to give the desired value of the total current. In Results the far-field analysis is illustrated by a simple example that admits an exact solution of the Boundary Layer Model. The far-field behavior of this solution is in complete agreement with our conclusions obtained from the Boundary Surface Model. The simple example is then used to illustrate the numerical method, which is finally applied to obtain far-field solutions under the experimental conditions of Bell and Miller (1984).

METHODS

Construction of Boundary Surface Model

In this section we obtain the Boundary Surface Model from a discrete-time, discrete-state random walk on a cubic lattice. The mathematical theory of random walks converging to diffusion processes is discussed, for example, by Karlin and Taylor (1981). This technique was used by Berg and Purcell (1977) in their treatment of surface diffusion, and more recently by McGill and Schumaker (1996) to construct boundary conditions for single ion diffusion.

Consider the cubic volume $0 \le X, Y, Z \le L$, with lattice sites at locations iL/n, jL/n, and kL/n, where indices i and $j \in \{1, 2, \ldots, n\}$ and $k \in \{0, \ldots, n\}$. We will refer to the square sublattices associated with each fixed k as *levels*. The level $k = 0$ represents the boundary surface, and each lattice site on that level corresponds to an area $(L/n)^2$. The levels $k \ge 1$ represent the bulk solution, and each lattice site on these levels corresponds to a volume $(L/n)^3$.

Let $P_{i,j,k}(t)$ be the probability that the lattice site (i, j, k) is occupied by a random walker at time t. Lattice site probabilities can be related to concentrations of random walkers in the bulk $C^b_{i,j,k}$ and on the surface $C^s_{i,j}$ according to

$$P_{i,j,0}(t) = C^s_{i,j}(t)L^2n^{-2}, \quad (6)$$

$$P_{i,j,k}(t) = C^b_{i,j,k}(t)L^3n^{-3}, \quad (7)$$

for $i, j, k \ge 1$. Alternatively, the concentrations may be expressed using the notation

$$C^s_{i,j}(t) = C_s(X_i, Y_j, t), \quad (8)$$

$$C^b_{i,j,k}(t) = C_b(X_i, Y_j, Z_k, t), \quad (9)$$

where $X_i = i/n$, $Y_j = j/n$ and $Z_k = k/n$.

Random walkers step between nearest-neighbor lattice sites at discrete time intervals Δt. There will be four different transition probabilities. A walker may take a step between lattice sites in the bulk solution with probability γ_b. A step may be taken between sites on the boundary surface with probability γ_s. Steps occur from the bulk (level 1) to the surface with probability γ_{bs} and from the surface to bulk with probability γ_{sb}. These transition probabilities are defined according to

$$\gamma_b = \Delta t D L^{-2} n^2, \quad (10)$$

$$\gamma_s = \Delta t D L^{-2} n^2, \quad (11)$$

$$\gamma_{bs} = \Delta t K_{bs} L^{-1} n. \quad (12)$$

$$\gamma_{sb} = \Delta t K_{sb}. \quad (13)$$

In the diffusion limit that follows, $n \to \infty$. So that transition probabilities never sum to a value greater than one, the time step must also scale with n:

$$\Delta t = \Delta\tau / n^2. \quad (14)$$

We must now analyze three cases, corresponding to time evolution on levels $k = 0$, $k = 1$, and $k > 1$.

Consider a lattice site in the interior of the bulk solution, with $k > 1$. A walker on this site may step to one of six adjoining sites with probability γ_b. On the other hand, the lattice site may receive a walker from one of the six adjoining sites. According to these rules, the time evolution of an interior lattice site is given by

$$\begin{aligned} P_{i,j,k}(t + \Delta t) - P_{i,j,k}(t) &= [P_{i+1,j,k}(t) + P_{i-1,j,k}(t) - 2P_{i,j,k}(t)]\gamma_b \\ &+ [P_{i,j+1,k}(t) + P_{i,j-1,k}(t) - 2P_{i,j,k}(t)]\gamma_b \\ &+ [P_{i,j,k+1}(t) + P_{i,j,k-1}(t) - 2P_{i,j,k}(t)]\gamma_b. \end{aligned} \quad (15)$$

Now substitute the definition of the bulk concentration, Eq. 7, and transition probability γ_b, Eq. 10. Divide through by $L^3n^{-3}\Delta t$. On the left-hand side we obtain a familiar difference quotient whose limit as $n \to \infty$ is a time derivative. The right-hand side is a sum of 3-second differences. Let $n \to \infty$, scaling $i, j, k \to \infty$ in such a way that $X_i \to X$, $Y_j \to Y$, and $Z_k \to Z$. We then obtain, for example,

$$\begin{aligned} \lim_{n\to\infty} L^{-2}n^2[C^b_{i+1,j,k}(t) + C^b_{i-1,j,k}(t) - 2C^b_{i,j,k}(t)] \\ = \frac{\partial^2}{\partial X^2} C_b(X, Y, Z). \end{aligned} \quad (16)$$

Evaluating these limits, we obtain the diffusion equation in

the bulk:

$$\frac{\partial C_b}{\partial t} = D\nabla^2 C. \tag{17}$$

Now consider a lattice site in the interior of the boundary surface, for which $k = 0$. A walker on this site may step to four adjoining sites on the boundary surface with probability γ_s, or to the adjoining site on level $k = 1$ with probability γ_{sb}. Walkers may also step in the reverse direction in each case, in particular, from level $k = 1$ with probability γ_{bs}. The time evolution of such a lattice site on the boundary surface is given by

$$\begin{aligned} P_{i,j,0}(t + \Delta t) - P_{i,j,0}(t) \\ = [P_{i+1,j,0}(t) + P_{i-1,j,0}(t) - 2P_{i,j,0}(t)]\gamma_s \\ +[P_{i,j+1,0}(t) + P_{i,j-1,0}(t) - 2P_{i,j,0}(t)]\gamma_s \\ +P_{i,j,1}(t)\gamma_{bs} - P_{i,j,0}(t)\gamma_{sb}. \end{aligned} \tag{18}$$

Substitute the definitions of the concentrations and transition probabilities. Divide through by $L^2 n^{-2}\Delta t$. Letting $n \to \infty$, and scaling i, j, and k as before, obtain

$$\frac{\partial C_s}{\partial t} = D\nabla^2 C_s + C_b(X, Y, 0, t)K_{bs} - C_s(X, Y, t)K_{sb}. \tag{19}$$

This is a diffusion equation for concentration on the surface, with an additional inhomogeneous term representing current flowing between the surface and the bulk.

Finally, consider a lattice site on level $k = 1$. A walker from this site may step to one of five neighboring sites in the bulk with probability γ_b or to a site on the surface with probability γ_{bs}. Walkers may also step in the reverse direction, from the surface with probability γ_{sb}. The time evolution is given by

$$\begin{aligned} P_{i,j,1}(t + \Delta t) - P_{i,j,1}(t) \\ = [P_{i+1,j,1}(t) + P_{i-1,j,1}(t) - 2P_{i,j,1}(t)]\gamma_b \\ +[P_{i,j+1,1}(t) + P_{i,j-1,1}(t) - 2P_{i,j,1}(t)]\gamma_b \\ +[P_{i,j,2}(t) - P_{i,j,1}(t)]\gamma_b \\ +P_{i,j,0}\gamma_{sb} - P_{i,j,1}\gamma_{bs}. \end{aligned} \tag{20}$$

Substitute definitions for the concentrations and transition probabilities. Divide through by $L^2 n^{-2}\Delta t$ and let $n \to \infty$, scaling i, j, and k as before. Only the last two terms on the right-hand side make nonzero contributions to this limit. Obtain

$$D\frac{\partial C_b}{\partial Z}(X, Y, 0, t) = C_b(X, Y, 0)K_{bs} - C_s(X, Y)K_{sb} \tag{21}$$

which expresses the flow of probability between the bulk and the surface in two different ways.

Equations 17, 19, and 21 form a time-dependent model for coupled bulk and boundary layer diffusion. We are interested only in steady-state currents to the ion channel entrances and set the time derivatives to zero. Transforming to cylindrical coordinates, we finally obtain Eqs. 2–4 in the Introduction.

Mean dwell time on boundary surface

The random walk construction also gives us insight into the behavior of trajectories on the surface in the Boundary Surface Model. In the following, we shall calculate the mean dwell time on the surface, ignoring the possibility that the diffuser is absorbed at the entrance region.

Consider a walker that first enters the boundary surface at a time t_0. The probability that it will leave the surface on the next time step is just γ_{sb}. The probability that the walker will remain on the surface for at least m further time steps is $(1 - \gamma_{sb})^m$. Let $t = m\Delta t$ be a fixed time interval, and now consider the diffusion limit $n \to \infty$ or $\Delta t \to 0$, according to Eq. 14. The probability that the walker will remain on the surface at least a fixed time t is given by

$$\lim_{m\to\infty}(1 - \gamma_{sb})^m = \lim_{\Delta t\to 0}(1 - \Delta t K_{sb})^{t/\Delta t} = e^{-K_{sb}t}, \tag{22}$$

where the limit can by evaluated by using L'Hôpital's rule. The mean duration of the trajectory on the surface is simply

$$\bar{T} = \int_0^\infty te^{-K_{sb}t}dt = K_{sb}^{-1}. \tag{23}$$

Choosing K_{bs} and K_{sb}

Far from the channel entrance, concentrations in the boundary layer will be close to equilibrium. In this section, K_{bs} and K_{sb} are chosen to give fluxes into and out of the boundary layer at equilibrium.

The ratio K_{bs}/K_{sb} is specified by considering Eq. 3 at equilibrium:

$$C_s^\infty K_{sb} = C_0 K_{bs}, \tag{24}$$

where C_0 is the limiting ion concentration in the bulk far from the channel entrance, and C_s^∞ is the integral over the equilibrium concentration in the boundary layer:

$$C_s^\infty = \int_0^{\zeta_0} C_0 e^{-\psi(\zeta)}d\zeta. \tag{25}$$

Introduce the boundary surface association constant $\kappa = K_{bs}/K_{sb}$, in analogy with a chemical equilibrium constant. The two previous equations may be immediately combined to see that κ is simply given by an integral over the Boltz-

mann factor:

$$\kappa = \int_0^{\zeta_0} e^{-\psi(\zeta)} d\zeta. \tag{26}$$

The mean dwell time in the 3D boundary layer $\hat{T}$ for an ion with initial coordinate ζ may be calculated as described in the Appendix. Weigh $\hat{T}$ by the equilibrium probability density in the boundary layer to determine K_{sb}:

$$K_{sb}^{-1} = (C_s^{\infty})^{-1} \int_0^{\zeta_0} C_0 \exp(-\psi(\zeta)) \hat{T}(\zeta) d\zeta. \tag{27}$$

The calculation of $\hat{T}(\zeta)$ in the Appendix assumes that trajectories reflect off the physical membrane surface without delay, an assumption equivalent to calculating the mean escape time using the even extension of the potential profile, as shown in Fig. 2.

Far-field analysis

This section obtains a partial solution of the Boundary Surface Model that is valid in the "far field," far from the channel entrance. C_b satisfies Eq. 2. Far from the channel entrance, $C_b \to C_0$. We therefore begin by considering the most general form of a solution of Laplace's equation with azimuthal symmetry satisfying these boundary conditions (see, for example, Jackson, 1975):

$$C_b(r, \theta) = C_0 + \sum_{m=0}^{\infty} B_m r^{-(m+1)} L_m(\cos \theta), \tag{28}$$

where $r = (X^2 + Y^2 + Z^2)^{1/2}$ and $\cos \theta = Z/r$. In cylindrical coordinates,

$$C_b(\rho, Z) = C_0 + \sum_{m=0}^{\infty} B_m (\rho^2 + Z^2)^{-(m+1)/2} L_m(\xi(\rho, Z)), \tag{29}$$

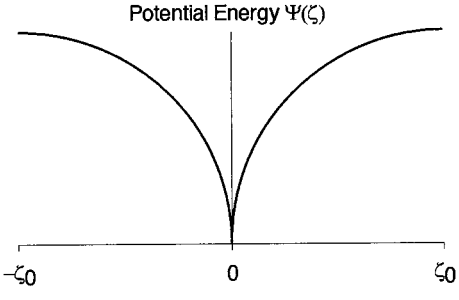

FIGURE 2 Even extension of potential energy profile, giving the energy of ions as a function of distance from the membrane. The boundary layer is in the interval $0 \le \zeta \le \zeta_0$. The mean dwell time $\hat{T}$ of an ion in the extended boundary layer is the same as the dwell time in the boundary layer, assuming specular reflection at the membrane surface.

where $\xi(\rho, Z) = Z(\rho^2 + Z^2)^{-1/2}$. L_m denotes the Legendre polynomial of order m.

We must now calculate $(\partial/\partial Z)C_b(\rho, 0)$ and $C_s(\rho)$ to made use of Eq. 3. To differentiate the Legendre polynomial, use the recurrence relation (Jackson, 1975)

$$(\xi^2 - 1) \frac{d}{d\xi} L_m(\xi) = m\xi L_m(\xi) - m L_{m-1}(\xi). \tag{30}$$

Then by differentiating, setting $Z = 0$, and finally simplifying, obtain

$$\frac{\partial}{\partial Z} C_b(\rho, 0) = \sum_{m=0}^{\infty} B_m \rho^{-(m+2)} m L_{m-1}(0). \tag{31}$$

Legendre polynomials have the property that $L_{2m+1}(0) = 0$. Thus

$$\frac{\partial}{\partial Z} C_b(\rho, 0) = \sum_{k=0}^{\infty} B_{2k+1} \rho^{-(2k+3)} (2k+1) L_{2k}(0). \tag{32}$$

Combining Eqs. 3 and 4 and writing ∇^2 in polar coordinates,

$$D \frac{1}{\rho} \frac{d}{d\rho} \rho \frac{d}{d\rho} C_s = -D \frac{\partial}{\partial Z} C_b(\rho, 0). \tag{33}$$

Substitute Eq. 32 and integrate twice to obtain

$$C_s(\rho) = \sum_{k=0}^{\infty} B_{2k+1} \frac{\rho^{-(2k+1)}}{-(2k+1)} L_{2k}(0) + K_1 \ln \rho + K_2. \tag{34}$$

Because $C_s \to C_s^{\infty}$ as $\rho \to \infty$, we must have $K_1 = 0$ and $K_2 = C_s^{\infty} = C_0\kappa$, where the last expression is given by Eq. 24. With the exception of the constant term, C_s depends only on odd powers of ρ^{-1}.

Substitute into Eq. 3 our results: Eq. 29 with $Z = 0$, and Eqs. 32 and 34. Identify the coefficients of ρ^{-n} on either side of the equation; we have for $n = 1$:

$$B_1 = -\kappa B_0. \tag{35}$$

κ has units of length. It is convenient to express B_0 and B_1 in terms of a new quantity. Let

$$B_0 = -bC_0, \tag{36}$$

where $b > 0$, and b has units of length. If we now make use of this result in Eqs. 28 and 34, and using $L_0(\cos \theta) = 1$ and $L_1(\cos \theta) = \cos \theta$, we finally obtain the following far-field expressions:

$$C_b(r, \theta) = C_0 \left[1 - \frac{b}{r} + \frac{\kappa b}{r^2} \cos \theta + \mathcal{O}(r^{-3}) \right], \tag{37}$$

$$C_s(\rho) = C_0 \kappa \left[1 - \frac{b}{\rho} + \mathcal{O}(\rho^{-3}) \right]. \tag{38}$$

From the dependence of both C_b on $1 - b/r$ and C_s on $1 - b/\rho$, we may consider b as the effective capture radius of the

channel in the far field. The surface concentration C_s is proportional to the boundary surface association constant given by Eq. 26. κ increases with both the thickness of the boundary layer ζ_0 and the depth of the electrical potential ψ. A corresponding term proportional to κ modulates the bulk concentration field in Eq. 37.

Further insight into the far-field solution can be gained by calculating far-field expressions for ion fluxes in the bulk and on the surface. From Fick's law,

$$\begin{aligned}\mathbf{J}_b &= -D\nabla C_b \\ &= -DC_0 b\left[\frac{1}{r^2} - \frac{2\kappa}{r^3}\cos\theta + \mathbb{O}(r^{-4})\right]\hat{\mathbf{e}}_r \\ &\quad + DC_0 b\left[\frac{\kappa}{r^3}\sin\theta + \mathbb{O}(r^{-4})\right]\hat{\mathbf{e}}_\theta,\end{aligned} \tag{39}$$

$$\begin{aligned}\mathbf{J}_s &= -D\nabla C_s \\ &= -DC_0 b\kappa\frac{1}{\rho^2}\hat{\mathbf{e}}_\rho + \mathbb{O}(\rho^{-4}).\end{aligned} \tag{40}$$

where $\hat{\mathbf{e}}_r$, $\hat{\mathbf{e}}_\theta$, and $\hat{\mathbf{e}}_\rho$ are unit vectors in the direction of increasing r, θ, and ρ, respectively.

An analogy with the electrostatic multipole expansion may be useful in visualizing this result. The second term of Eq. 37 is analogous to the monopole contribution to an electrostatic potential. Its contribution to the flux $\mathbf{J}_b$ corresponds to an electric field directed radially inward, toward the channel entrance. The third term of Eq. 37 is analogous to a dipole contribution of strength κb oriented in the direction of the positive Z axis. The resultant flux density, evaluated at $Z = 0$, is into the plane of the membrane. The surface flux is directed radially inward, toward the channel. Its magnitude increases as ρ^{-2} as ρ decreases. The global picture is that of an ion flux toward the channel, and from the bulk phase to the boundary surface.

The total flux into the channel may be computed as the total flux directed inward through a hemisphere, centered on the channel, and of radius r_0. The integrated flux passing into the hemisphere through the bulk medium, F_b, may be computed from the far-field expression for the bulk flux density, Eq. 39:

$$\begin{aligned}F_b &= 2\pi\int_0^{\pi/2}\mathbf{J}_b\cdot\hat{\mathbf{e}}_r\sin\theta\, r_0^2\,d\theta \\ &= -2\pi DC_0 b(1 - \kappa r_0^{-1}) + \mathbb{O}(r_0^{-2}).\end{aligned} \tag{41}$$

The hemisphere intersects the boundary surface on a circle of radius r_0. The integrated flux passing into the hemisphere through this circle may be computed from the far-field expression for the surface flux density,

$$\begin{aligned}F_s &= 2\pi r_0\mathbf{J}_s\cdot\hat{\mathbf{e}}_\rho \\ &= -2\pi DC_0\kappa b r_0^{-1} + \mathbb{O}(r_0^{-3}).\end{aligned} \tag{42}$$

The total flux into the hemisphere, including the circle at its base, is the sum of these two components. Note that the terms of order r_0^{-1} shown explicitly in Eqs. 41 and 42 cancel. The random walk construction of the boundary surface model shows that it describes a time-stationary state of coupled two- and three-dimensional diffusions. It follows that the flux into a hemisphere of radius r_0 must be independent of r_0, and we conclude that the total flux F_T is given by

$$F_T = -2\pi DC_0 b, \tag{43}$$

where the minus sign reflects the fact that the flux is directed into the hemisphere. This is exactly the expression for the total flux into a hemispherical sink of radius b in the absence of boundary layer diffusion (see, for example, Hille, 1992).

Finally note that the expression for F_s is obtained from a differentiation and integration of the expression for $C_s(\rho)$. As noted below Eq. 34, the powers series for $C_s(\rho)$ includes only the constant term and odd powers of ρ^{-1}. It follows that the series for F_s only includes odd powers of $\rho^{-1} = r_0^{-1}$. So that this series may be added to that for F_b to obtain the result Eq. 43, all even powers of r_0^{-1} of order 2 and higher in the series for F_b must vanish. When the corresponding terms are nonzero in the expression for J_b, the integral in Eq. 41 must vanish. We may therefore replace the symbol $\mathbb{O}(r_0^{-2})$ in Eq. 41 with $\mathbb{O}(r_0^{-3})$.

Boundary conditions from the far-field solution

The next section describes numerical integration of the Boundary Surface Model on a rectangular domain in cylindrical coordinates: $0 \le \rho \le \rho_{max}$ and $0 \le Z \le Z_{max}$. The channel entrance is at the origin. One significant problem is the specification of appropriate boundary conditions at ρ_{max} and Z_{max}. The far-field analysis can provide appropriate boundary conditions.

Truncation of the far-field result, Eqs. 37 and 38, to eliminate the $\mathbb{O}(r^{-3})$ and $\mathbb{O}(\rho^{-3})$ terms, yields the *dipole approximation*. Consider first the truncation of Eq. 37, written in cylindrical coordinates:

$$C_b(\rho, Z) = C_0[1 - b(\rho^2 + Z^2)^{-1/2} + \kappa bZ(\rho^2 + Z^2)^{-3/2}]. \tag{44}$$

Assuming that κ is specified, only b remains unknown. Eliminating b between this equation and its derivative with respect to Z, obtain

$$\frac{\partial}{\partial Z}C_b + f(\rho, Z, \kappa)C_b = f(\rho, Z, \kappa)C_0, \tag{45}$$

where

$$f(\rho, Z, \kappa) = \frac{(Z + \kappa)(\rho^2 + Z^2) - 3\kappa Z^2}{(\rho^2 + Z^2)(\rho^2 + Z^2 - \kappa Z)}. \tag{46}$$

These equations provide a boundary condition at $Z = Z_{max}$.

The unknown b can also be eliminated between Eq. 44 and its derivative with respect to ρ. This yields

$$\frac{\partial}{\partial \rho} C_b + g(\rho, Z, \kappa) C_b = g(\rho, Z, \kappa) C_0, \tag{47}$$

where

$$g(\rho, Z, \kappa) = \frac{\rho(\rho^2 + Z^2) - 3\kappa\rho Z}{(\rho^2 + Z^2)(\rho^2 + Z^2 - \kappa Z)}. \tag{48}$$

These equations provide a boundary condition at $\rho = \rho_{max}$.

Finally, Eq. 38 can be used to obtain a boundary condition on the boundary surface, at $\rho = \rho_{max}$. Begin with the truncation obtained by neglecting the $\mathbb{O}(\rho^{-3})$ terms. Differentiate and eliminate b to find

$$\frac{\mathrm{d}}{\mathrm{d}\rho} C_s + \frac{1}{\rho} C_s = \frac{1}{\rho} C_0 \kappa. \tag{49}$$

These boundary conditions are exactly satisfied by the dipole approximation. and are useful for numerical integration when ρ_{max} and Z_{max} are so large that the terms $\mathbb{O}(r^{-3})$ and $\mathbb{O}(\rho^{-3})$ in Eqs. 37 and 38 may be neglected.

A lower bound for ρ_{max} and Z_{max} is determined by the zeros of the numerators and denominators of f and g. These zeros reflect an unphysical extremum of the dipole approximation of Eq. 37 when r is small. If numerical integration is performed with $\rho_{max} = Z_{max}$, positivity of the numerators and denominators requires $Z_{max} > 2\kappa$.

Numerical solution of the Boundary Surface Model

This section describes an algorithm for numerically integrating the Boundary Surface Model. Unlike the dipole approximation, the Boundary Surface Model has no singularity at the channel entrance. It provides a better representation of the Boundary Layer Model at intermediate length scales.

Even the full Boundary Surface Model cannot give an accurate representation of the physical flow field close to the channel entrance. The values of K_{bs} and K_{sb} used in Eqs. 3 and 4 are obtained by assuming a Boltzmann distribution of concentrations in the boundary layer. Close to the channel, the actual distribution will depend on the detailed kinetics of ion entrance.

To proceed with the numerical solution, first introduce dimensionless coordinates $x = X/a$, $y = Y/a$, $z = Z/a$ and concentrations $c_b = C_b/C_0$ and $c_s = C_s/(aC_0)$. Substituting these definitions into Eqs. 2–4, one obtains

$$\nabla^2 c_b(\hat{\rho}, z) = 0, \tag{50}$$

$$\nabla^2 c_s(\hat{\rho}) = c_s(\hat{\rho}) k_{sb} - c_b(\hat{\rho}, 0) k_{bs}.$$

$$= -\frac{\partial}{\partial z} c_b(\hat{\rho}, 0), \tag{51}$$

where $\hat{\rho} = (x^2 + y^2)^{1/2}$. These cylindrical coordinates are used by the numerical integration. Dimensionless rate constants have also been introduced:

$$k_{bs} = aK_{bs}/D \qquad \text{and} \qquad k_{sb} = a^2 K_{sb}/D, \tag{52}$$

where $D = 1.96 \times 10^{-9}$ m^2 s^{-1} is the aqueous diffusion coefficient of K^+ (Hille, 1992), and $a = 4$ Å was chosen for numerical convenience.

Equations 50 and 51 are solved numerically, using Gauss-Seidel iteration on a 256 by 256 square lattice with two additional rows, as depicted in Fig. 3. Values of c_b are computed on the square lattice itself, whereas values of c_s are computed on the surface row shown below the lattice. In the normalized units described above, the lattice spacing is $h = 2/3$. The radius of the entrance region is 1, and therefore only the first two points of the surface row fall within the entrance region.

An accurate representation of the entrance region is not important for our purposes. The dipole approximation of the far-field expansion only depends on the boundary conditions at the entrance region through the parameter b. From Eq. 43, we see that b is proportional to the total flux into the channel. For the purpose of comparison with experiment, values of b can therefore by obtained from current measurements. The value of K_{se} in Eq. 5 is then adjusted to give the appropriate current.

The far-field boundary conditions, Eqs. 45, 47 and 49, are applied at the boundaries $\hat{\rho} = \hat{\rho}_{max}$ and $z = z_{max}$. These equations were obtained by eliminating the far-field capture radius b in the dipole approximation. However, estimates of b can be recovered from the values of c_b at the far bound-

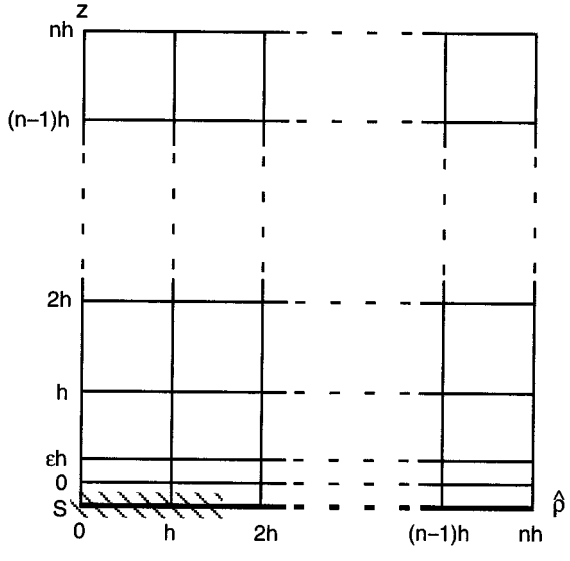

FIGURE 3 Lattice for numerical solution of the Boundary Surface Model. The bulk is represented on an $n + 1$ by $n + 1$ square lattice with lattice spacing h. $n = 255$ for the calculations presented in the text. z and $\hat{\rho}$ are dimensionless cylindrical coordinates described in the text. The additional row marked ϵh aids in the evaluation of a derivative at $z = 0$. The row S represents the boundary surface. The channel entrance is represented by the first two nodes of the S row (*hashed region*).

aries. If $\hat{\rho}_{max}$ and z_{max} are chosen to be large enough that the dipole approximation is accurate at the far boundaries, then similar estimates of b can be made at all points along these boundaries.

This observation has been incorporated into a consistency check for the numerical integration. Estimates of b are calculated at four uniformly spaced points along the boundary $\hat{\rho} = \hat{\rho}_{max}$ and at four uniformly spaced points along the boundary $z = z_{max}$. Additional estimates of b are calculated at the intersection of the ϵ and surface rows with the boundary $\hat{\rho} = \hat{\rho}_{max}$. Empirically, we find that $\rho_{max} = Z_{max} > 10\kappa$ gives reasonably consistent results.

All finite differences are computed with symmetrized formulas whose accuracy improves as $\mathbb{O}(h^2)$, except on the boundaries $\hat{\rho} = \hat{\rho}_{max}$, $z = z_{max}$, and $z = 0$, where first-order formulas are used. A relatively accurate first-order finite-difference approximation to the partial derivative with respect to z appearing in Eq. 51 was computed with the aid of an additional row of points placed on the lattice at $z = \epsilon h$. For the results presented here, $\epsilon = 0.1$.

RESULTS

Far-field expansion for an absorbing hemisphere

In this section we consider the example of a hemispherical absorber of radius s_0 centered at the origin in the absence of an electrical potential. Fig. 4 illustrates the geometry. The solution C_p of the Boundary Layer Model, Eq. 1, will be identified with the bulk concentration C_b of the Boundary Surface Model for $Z = \zeta - \zeta_0 > 0$. The integral of C_p over the interval $0 < \zeta < \zeta_0$ will be identified with the surface concentration C_s of the Boundary Surface Model. Complete agreement will be obtained with the form of the far-field expansions, Eqs. 37 and 38.

To begin, setting $\psi = 0$ in Eq. 1 gives Laplace's equation. The well-known solution

$$C_p = C_0\left(1 - \frac{s_0}{s}\right) \tag{53}$$

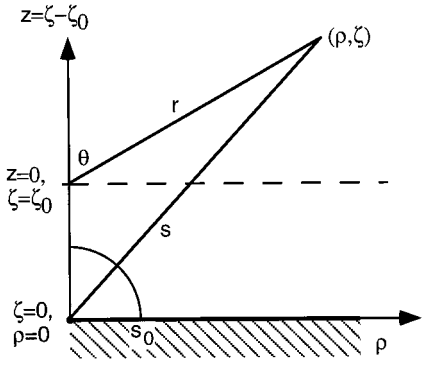

FIGURE 4 Boundary Layer Model and Boundary Surface Model coordinate systems. The origin of the Boundary Layer Model is on the membrane surface at $\zeta = 0$. The origin of the Boundary Surface Model is above, at the interface between the bulk and the boundary layer. The text discusses a simple example in which an absorbing hemisphere of radius s_0 models the ion channel entrance.

satisfies the boundary conditions $C_p = 0$ for $s = s_0$ and $C_p \to C_0$ as $s \to \infty$. Transform the solution to the spherical coordinates (r, θ) of the Boundary Surface Model and expand in inverse powers of r to obtain

$$C_p = C_0\left[1 - \frac{s_0}{r} + \frac{s_0\zeta_0}{r^2}\cos\theta + \mathbb{O}(r^{-3})\right]. \tag{54}$$

For $\psi = 0$ we have, according to Eq. 26, $\kappa = \zeta_0$. Identifying $b = s_0$, this form agrees with the explicit terms in the far-field expansion, Eq. 37.

Now consider the higher order terms of C_p in the bulk region $Z > 0$. Because of azimuthal symmetry, C_p has the form given by the right-hand side of Eq. 28. The bulk flux density J_b is obtained from Eq. 39. The bulk current F_b through a hemisphere of radius r_0 and centered at the origin $r = 0$ is given by Eq. 41. For $m > 0$ and even, we have the identity

$$\int_0^{\pi/2} L_m(\cos\theta)\sin\theta\,d\theta = 0. \tag{55}$$

and it follows that all even powers of r^{-1} of order 2 or higher vanish in the series for F_b. This conclusion agrees with the discussion after Eq. 43.

C_s may be constructed by transforming Eq. 53 to cylindrical coordinates and integrating over the interval $0 < \zeta < \zeta_0$. Obtain

$$\begin{aligned} C_s &= C_0[\zeta_0 - s_0\sinh^{-1}(\zeta_0/\rho)] \\ &= C_0\zeta_0\left[1 - \frac{s_0}{\rho} + \frac{1}{6}\frac{s_0\zeta_0^2}{\rho^3} + \mathbb{O}(\rho^{-5})\right], \end{aligned} \tag{56}$$

Identifying $b = s_0$, this agrees with the form of Eq. 38. Because $\sinh^{-1}$ is an odd function of its argument, the series for C_s only contains the constant term and odd powers of ρ^{-1}.

We cannot generally expect perfect agreement between the Boundary Layer Model and the far-field expansion of the Boundary Surface Model when $\psi \neq 0$. The form of the expansion depends on the parameter κ, which in turn depends on both ψ and the choice of ζ_0. For a given choice of ζ_0, the Boundary Surface Model neglects the electrical potential outside the boundary layer. However, this error can be made small with an appropriate choice for ζ_0.

Boundary Surface Model for an absorbing hemisphere

In this section we discuss the numerical solution of the Boundary Surface Model corresponding to the hemisphere example. Parameters are chosen to match the experimental conditions of Bell and Miller (1984) at 200 mM $[K^+]$ for the purpose of later comparison.

The boundary layer thickness is taken to be $\zeta_0 = 3\lambda_D = 2.06$ nm, where λ_D is the Debye length. For the numerical

solution, parameter K_{se} appearing in Eq. 5 was adjusted empirically to give a current matching the experimental value of 12.8 pA at 60 mV applied potential. To represent the hemispherical model, K_{bs} and K_{sb} were calculated assuming the membrane potential $\psi = 0$; their values are given in the caption of Fig. 5. Details of the numerical integration are described in the Methods section. The far-field capture radius corresponding to the experimental current is $b = 0.538$ Å, according to Eq. 43. This value was used in representations of the dipole approximation (the far-field expansion truncated after order r^{-2}; see Eq. 37).

Fig. 5 shows normalized K^+ concentrations at the interface between the boundary layer and the bulk region. The solid curve corresponds to the exact solution of the hemisphere example, and filled circles correspond to the numerical solution of the Boundary Surface Model. These latter are values of concentrations calculated at the nodes of the row $z = 0$ in Fig. 3. Concentration values corresponding to the first nine nodes (calculated at $\hat{\rho} = 0, h, \ldots 8h$) are shown in Fig. 5 and then every fourth concentration thereafter. The dashed line gives the dipole approximation.

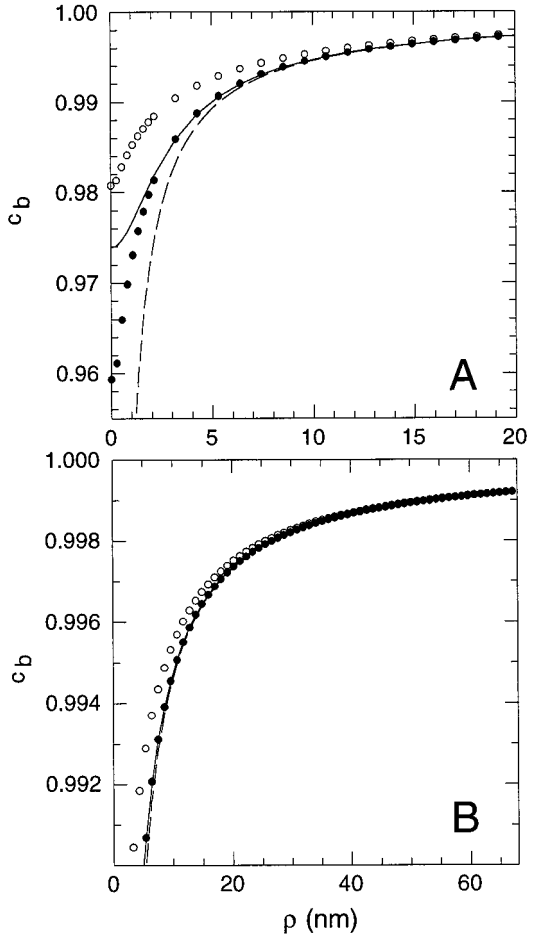

FIGURE 5 Normalized bulk concentrations at the interface with the boundary surface, $Z = 0$. $c_b = C_b/C_0$. The solid curve shows the exact solution for the hemisphere example. Filled circles give the numerical solution of the Boundary Surface Model for the hemisphere example. Open circles show the numerical solution of the Bell and Miller example. The dashed curve gives the dipole approximation, which is the same for these two examples when $Z = 0$. (*A*) Concentrations close to the channel entrance. (*B*) Concentrations in the far field. Rate constants for the hemisphere example are $K_{bs} = 2.85$ m s^{-1} and $K_{sb} = 1.38 \times 10^9$ s^{-1}. Those for the Bell and Miller example are $K_{bs} = 2.52$ m s^{-1} and $K_{sb} = 3.96 \times 10^8$ s^{-1}.

Fig. 5 *A* details the concentration field within 20 nm of the channel entrance. The Boundary Surface Model does not follow the hemisphere solution close to the channel entrance. However, boundary surface concentrations agree well with the exact solution for $\rho > 3$ nm. The dipole approximation gives concentrations in good agreement with the exact solution for $\rho > 10$ nm. Fig. 5 *B* gives an expanded view of the concentration differences over the whole domain of the numerical integration. Both the Boundary Surface Model and the dipole approximation follow the exact solution very closely in the far field.

Fig. 6 *A* compares curves of constant concentration for the exact solution of the hemispherical absorber with those of the numerical solution and the dipole approximation. Concentrations shown along the line $Z = 0$ correspond to Fig. 5. The flux $\mathbf{J}_b$ is locally orthogonal to the level curves, and is directed radially toward the hemisphere 2 nm below the origin. Level curves given by the dipole approximation of the Boundary Surface Model cannot be distinguished from those of the hemisphere example. Level curves for the numerical results are just inside the others because of a slightly smaller total flux.

Fig. 7 shows the Z component of the bulk flux density $\mathbf{J}_b = -D\nabla C_b$ integrated azimuthally and evaluated at $Z = 0$. This is the distribution of integrated current flow from the bulk to the boundary layer as a function of ρ. Flux densities are zero at the origin, reflecting the integration around the radial angle. The area under this distribution, including the tail $\rho > \rho_{max}$, is equal to the total flux into the channel. Therefore, the same area is found under the curves corresponding to the exact solution of the hemisphere problem and the numerical solution of the corresponding Boundary Surface Model. Close to the channel entrance, the computed flux into the boundary surface of the numerical solution is greater than the corresponding flux into the boundary layer of the hemisphere solution. Compensating this excess, there is a region further from the entrance region where the hemisphere flux density is greater.

In contrast to the differences found close to the channel entrance, for $\rho > 10$ nm the two flux densities are in good agreement. Fig. 7 *B* gives an expanded view of the solution in the far field. For $22 < \rho < 61$ nm, the amplitudes of the hemisphere and Boundary Surface flux densities agree to within 1%. Close to the boundary of the domain of numerical integration, the numerical flux density begins to exceed that of the hemisphere solution, and is finally greater by 2.5% at $\rho = \rho_{max}$. A possible source of numerical error is the first-order finite-difference formulas used at the boundaries $\hat{\rho} = \hat{\rho}_{max}$ and $z = z_{max}$, as described in the Methods section.

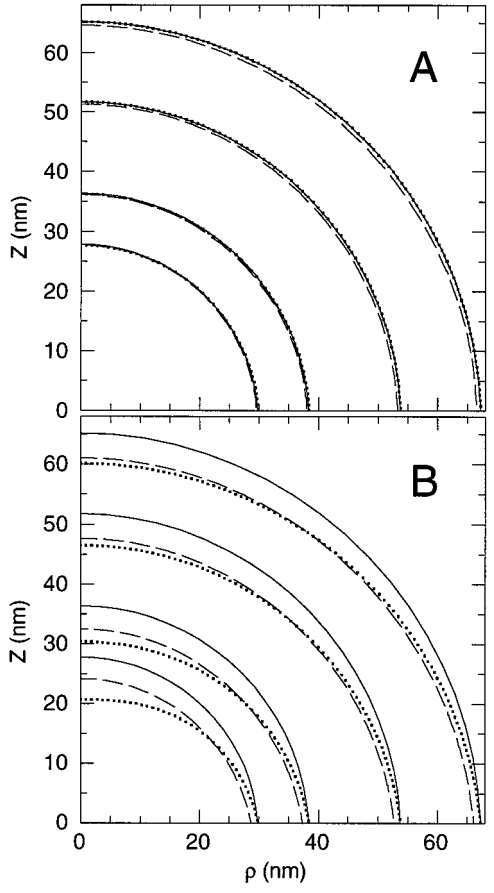

FIGURE 6 Level curves of bulk concentrations. Each figure shows four sets of level curves corresponding to normalized concentrations C_b/C_0 = 0.9982, 0.9986, 0.9990, and 0.9992, listed in order from the origin. In both figures, the solid curves show the exact solution for the hemisphere example. (*A*) The dashed curves show the numerical solution for the hemisphere Boundary Surface Model, and the dotted curves give the dipole approximation. The latter very nearly coincide with the exact solution. (*B*) The dashed curves show the numerical solution for the Bell and Miller example, and the dotted curves indicate the corresponding dipole approximation. Note the separation between these two sets of curves and the hemisphere solutions near the *Z* axis.

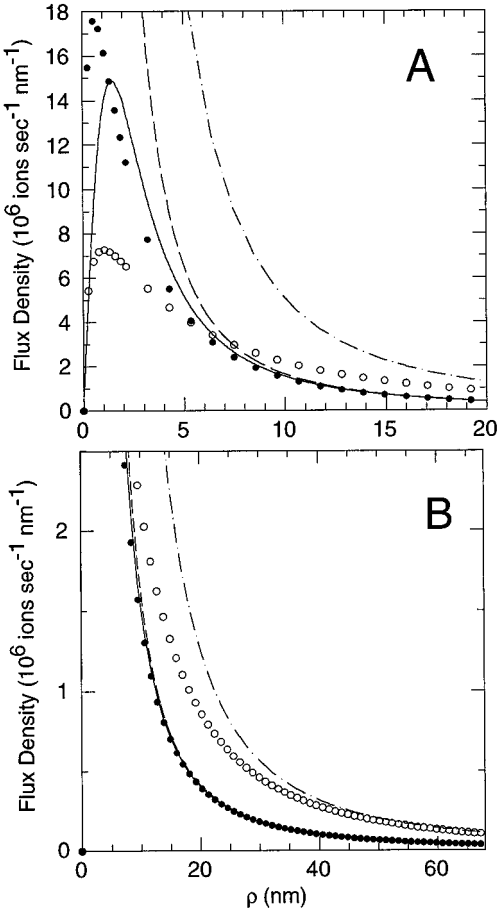

FIGURE 7 Integrated flux densities from bulk to surface. Curves show $2\pi\rho J_z(\rho, 0)$, where $J_z(\rho, 0)$ is the *Z* component of the bulk flux density evaluated at the interface between the bulk and the boundary layer. Solid curves give the exact solution of the hemisphere example. Filled circles show the corresponding numerical solution, and the dashed curve gives the dipole approximation. Open circles give the numerical solution for the Bell and Miller example, and the dot-dashed curves give the corresponding dipole approximation. (*A*) Flux densities close to the channel entrance. (*B*) Flux densities in the far field.

Fig. 8 shows the integrated flux $F_s = 2\pi\rho|\mathbf{J}_s|$ in the boundary layer or boundary surface as a function of ρ. The small difference in surface flux between the hemisphere and numerical solution near $\rho = 0$ is due to the different flux directly into the entrance region from the bulk. The two solutions agree very closely in the far field. For $\rho > 12$ nm, the numerical flux is within 2% of the hemisphere solution. In the interval $20 < \rho < 58$ nm, the relative difference is less than 1%.

Boundary Surface Model of Bell and Miller experiments

Bell and Miller (1984) measured K^+ currents through sarcoplasmic recticulum K^+ channels reconstituted in neutral and negatively charged lipid bilayers. The negatively charged bilayers were a 70% phosphatidylserine/30% phosphatidylethanolamine mixture with a measured charge density of $0.9 \pm 0.2e_0/nm^2$. We use $1.0e_0/nm^2$. Measurements were taken using symmetrical solutions in which K^+ was the sole cation and the major anion was gluconate. We consider the experimental conditions at $C_0 = 200$ mM K^+. The conductance estimated from their Fig. 2 *A* was ~213 ps, corresponding to a current of 12.8 pA at a transmembrane potential of 60 mV.

Following Bell and Miller, we modeled the electrical potential using nonlinear uni-univalent Gouy-Chapman-Stern theory (McLaughlin, 1977). This theory incorporates partial neutralization of the membrane due to association of K^+ with negative charges on the membrane. The binding is assumed to have a Langmuir form, with the experimentally determined association constant $K_a = 0.15$ M^{-1} (Eisenberg et al., 1979). Electrical potential values in the boundary layer range from $\Psi = -74$ mV at $\zeta = 0$ to $\Psi = -3$ mV at $\zeta = \zeta_0 = 3\lambda_D = 2.06$ nm. The electrical potential decays slightly faster than exponentially with length constant λ_D.

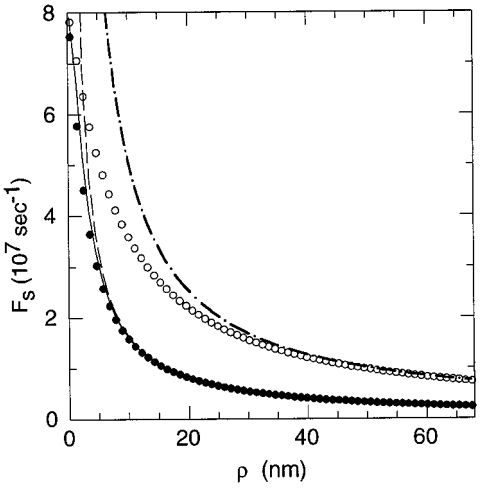

FIGURE 8 Surface flux F_s as a function of ρ. $F_s = 2\pi\rho J_s$, where J_s is the magnitude of the surface flux density. The solid curve shows the exact hemisphere solution, the filled circles the corresponding numerical solution, and the dashed curve the dipole approximation. The open circles show the numerical solution of the Bell and Miller example, and the dot-dashed curve shows the corresponding dipole approximation.

Boundary Surface rate constants K_{bs} and K_{sb} were calculated from the electrical potential profile as described in the Methods section. Their values are given in the caption of Fig. 5. The boundary surface association constant $\kappa = K_{bs}/K_{sb} = 6.36 \text{ nm} > 3\zeta_0$.

We have solved the Boundary Surface Model numerically using these parameters. The parameter K_{se} of Eq. 5 was adjusted to give the experimental current at 200 mM K^+. This model only contains information about the membrane and the total current under the conditions of Bell and Miller. There is no information about the structure of the sarcoplasmic recticulum K^+ channel. However, we shall refer to this as the Bell and Miller example.

Fig. 5 shows calculated concentrations at the interface between the bulk and boundary layer. The hemisphere example was constructed with the same total current F_T and thus, from Eq. 43, the same value of b as we are considering here. From Eq. 37, the dipole approximation is independent of κ at the interface, where $\theta = \pi/2$. Therefore, the dashed curve gives the dipole approximation for the present case as well as the hemisphere example. Indeed, the numerical solutions show that the computed Bell and Miller concentrations approach those of the dipole approximation as $\rho \rightarrow \rho_{max}$.

In Fig. 6 *B*, first consider the difference between the hemisphere example and the dipole approximation. These agree on the abscissa, where $\theta = \pi/2$. For smaller angles, the effect of the term proportional to κ in the dipole approximation is to flatten the level curves. The flux $\mathbf{J}_b$ is orthogonal to these. The dipole approximation flow field is directed into a broad segment of the boundary layer, instead of being radially directed into the channel entrance.

The level curves of the dipole approximation flatten close to the z axis. For those of the numerical solution of the Bell and Miller example, the flattening is less pronounced. This difference may be principally due to the $\mathbb{O}(r^{-3})$ term in the far-field expansion, Eq. 37, which depends upon the boundary conditions at the channel entrance. The angular distribution of the difference seems consistent with the requirement that the angular integral over the correction vanish in Eq. 41.

Fig. 7 shows the bulk flux density into the boundary surface, integrated around a circle of radius ρ, as a function of ρ. The significant difference between the hemisphere and Bell and Miller results is that, in the latter case, relatively more current enters the boundary surface at large ρ. In the far-field analysis, this can be seen in Eq. 39, where J_z is given by the term proportional to $\hat{\mathbf{e}}_\theta$ when evaluated at $\theta = \pi/2$. The ratio of the flux densities in the dipole approximation is proportional to κ(Bell and Miller)/κ (Hemisphere) ≈ 3.1. Numerically, the ratio approaches $\sim$2.9.

Finally consider again Fig. 8, showing surface current F_s as a function of ρ. The Bell and Miller example surface current has approximately the same intercept with the ordinate as the exact and numerical hemisphere example curves. This reflects the total current, which is nearly the same in the two examples, because $F_s \approx F_T$ for $\rho = a$. The ratio of the Bell and Miller to hemisphere surface currents approaches $\sim$3.0 at $\rho = \rho_{max}$. This ratio is consistent with Eq. 42, which shows that F_s is proportional to κ in the dipole approximation.

DISCUSSION

Relationship between boundary surface and boundary layer models

This paper provides an analysis of diffusive flow fields into an ion channel entrance under conditions in which an electric field attracts ions toward the membrane surface, and boundary layer diffusion may be important. To do this, the Boundary Layer Model of Fig. 1 *A* and Eq. 1 was reduced to the Boundary Surface Model of Fig. 1 *B* and Eqs. 2–4. These equations were solved simultaneously through $\mathbb{O}(r^{-2})$ and $\mathbb{O}(\rho^{-2})$ by applying only the equilibrium boundary conditions attained as $r \rightarrow \infty$ and $\rho \rightarrow \infty$. The single adjustable parameter, b, which appears in the solution to this order, was shown to be proportional to the total current, which may be measured experimentally. The resulting truncated dipole approximation was analyzed and compared with the numerical solution of the Boundary Surface Model.

The Boundary Surface Model is not mathematically equivalent to the Boundary Layer Model. Our method of reducing a 3D boundary layer to diffusion on a plane depends on modeling diffusive transport from the bulk to the surface by rate constants. The rate constants were adjusted to give the correct mean unidirectional fluxes in equilibrium, at which the distribution of ions in the surface layer is proportional to the Boltzmann factor $\exp(-\psi(\zeta))$. Close to the channel entrance, the equilibrium approximation will not be accurate. For given boundary conditions at

the channel entrance, one could discuss ρ-dependent K_{bs} and K_{sb}. We have no proof that these would not change the lowest order terms that enter into the dipole approximation.

However, we have demonstrated complete agreement of the solution of the hemisphere example with all of our conclusions concerning the far-field expansion, and, in particular, the terms that enter into the dipole approximation. We also have agreement in the case of one other exact example, that of an absorbing disk in the membrane (Smythe, 1968; Hall, 1975; unpublished results). Furthermore, our conclusions from the equilibrium expressions for K_{bs} and K_{sb} seem to be fully self-consistent and physically reasonable. Exact agreement between the Boundary Layer and Boundary Surface Models will not be obtained for nonzero ψ, because the latter model neglects fields extending outside the boundary layer. But this source of error is made small by an appropriate choice of the boundary layer thickness ζ_0.

Ion interactions with the membrane surface

There is experimental evidence that cations can pair directly with negative charges on the membrane surface, partially neutralizing the membrane surface charge density (Eisenberg et al., 1979). For this reason we followed Bell and Miller (1984) and calculated the electrical potential with Gouy-Chapman-Stern theory (McLaughlin, 1977), which provides for a Langmuir binding of ions to the membrane surface. However, we have not attempted to include such an interaction in the calculation of the mean dwell time in the boundary layer. Our analysis in the Appendix assumes specular reflection of ion trajectories at the membrane surface.

Interaction of ions with the membrane surface may also reduce their effective diffusion coefficient for motion parallel to the membrane in the boundary layer (Lifson, 1962). Direct binding of ions to the membrane surface would have this effect. Even without direct binding, discreteness of the membrane surface charge can roughen the effective surface potential if the mobile ions can approach the fixed charges too closely, or if the fixed charges are spaced too far apart (Nelson and McQuarrie, 1975).

The Boundary Surface Model can easily be modified to incorporate a reduced diffusion coefficient on the surface layer. One begins, in the random walk construction, by defining the transition probabilities γ_b and γ_s with distinct diffusion coefficients D_b and D_s. In the resulting boundary surface equations, the diffusion coefficient in the bulk is D_b, Eq. 3, and the diffusion coefficient on the surface is D_s, Eqs. 4 and 5.

The far-field analysis proceeds parallel to the discussion presented in the Methods section, with the result that the $\mathbb{O}(r^{-2})$ term in Eq. 37 is multiplied by an additional factor of D_s/D_b, but without any other changes in Eqs. 37 or 38. The bulk flux density is calculated using $\mathbf{J}_b = -D_b\nabla C_b$ in Eq. 39, and $J_s = -D_s\nabla C_s$ in Eq. 40. In the expressions for the resulting bulk flux density (Eq. 41), the first term is proportional to D_b, whereas the $\mathbb{O}(r_0^{-1})$ term is proportional to D_s. The $\mathbb{O}(r_0^{-1})$ term in the surface flux density (Eq. 42) is also proportional to D_s.

The effect of reducing the surface diffusion coefficient in the Boundary Surface Model, when the total current F_T is held constant, is to reduce the contribution of the surface current. This result suggests that direct ion binding to the membrane, discreteness of charge, or other factors that roughen the interaction potential of permeant ions near the membrane surface, will have the effect of reducing the current in the boundary layer.

Boundary layer diffusion and access resistance

One approach to modeling the influence of a charged membrane on conductance has been to assume that local concentrations of permeant ion in the vicinity of the channel entrance are enhanced by a Boltzmann factor, $C_p(\zeta) = C_0\exp(-\psi(\zeta))$, where ζ gives the height of the channel entrance above the plane of the membrane (Apell et al., 1979; Bell and Miller, 1984). From *IV* curves measured in neutral membranes, increased conductances are predicted by replacing bulk concentrations by the enhanced local concentrations. Implicit in this local concentration model is the assumption that the geometry of the flow into the channel entrance does not change greatly; concentrations in the region important to the channel are uniformly increased by the Boltzmann factor.

Using this local concentration approach, Bell and Miller constructed curves of predicted conductance as a function of bulk concentration C_0 for several different values of ζ. They found that measured conductances decreased, as C_0 decreased, more quickly than predicted by the local concentration model. See their Fig. 5.

Our results suggest that the geometry of the ion flux toward the channel entrance changes dramatically as C_0 decreases. At high bulk concentrations flux is directed into the channel with approximately spherical symmetry from the surrounding solution. At lower C_0, ion flux from the bulk is directed into a broad region of the boundary layer surrounding the channel. Within the boundary layer, there is a quasi-two-dimensional flux into the entrance.

The time-independent solution of the diffusion equation for a spherically symmetric flow into an absorbing center is given by Eq. 53. The corresponding 2D problem for a circularly symmetrical flow is given by Eq. 33, with zero on the right-hand side. The solution $C_s(\rho) = A + B \ln \rho$ does not satisfy the physical boundary conditions as $\rho \to \infty$. The more physical solution of the Boundary Surface Model depends on the flux density of ions into the surface from the bulk, as modeled by the right-hand side of Eq. 33. This flux density decreases as C_0 decreases. It is plausible that there is a region of depleted permeant ion concentration surrounding the channel entrance that deepens or widens as C_0 decreases. Such a local depletion may possibly explain the quickly decreasing conductances observed by Bell and Miller.

Apell et al. (1979) measured the effects of surface charge on C_s conductance through gramicidin in negatively

charged membranes. They also compared their measurements with a model assuming that local concentrations are enhanced by a Boltzmann factor. Somewhat similar to the results of Bell and Miller, they found that the measured conductance decreased slightly but significantly as bulk $[Cs^+]$ decreased. In contrast, over the entire range of their measurements, their model predicted local concentrations at the channel entrance far above the saturation concentration of the channel. It is plausible that their measurements may also be explained by a depleted region of ion concentration in the boundary layer near the channel entrance.

This proposed effect due to geometry is similar to the concept of access resistance, discussed in spherically symmetrical flows (for example, Läuger, 1976; Levitt, 1986; Chiu and Jakobsson, 1989). The Boundary Surface Model does not accurately depict ion flows in the immediate vicinity of the channel. A more detailed numerical study may be required to estimate the importance of any increased access resistance associated with the quasi-two-dimensional geometry of surface diffusion at low C_0.

APPENDIX

Mean time to escape the potential well

In this section we obtain a formula for the mean time to escape the potential energy well associated with the boundary layer. We require this to calculate K_{bs} and K_{sb}. The formula is a standard result in the theory of stochastic processes (e.g., Karlin and Taylor, 1981; Risken, 1989). Here we show that it can be obtained in a straightforward way by taking the diffusion limit of an appropriate random walk. This derivation is in the spirit of Berg and Purcell (1977).

We assume that the boundary layer extends over the interval $0 \le \zeta \le \zeta_0$. Let $\Psi(\zeta)$ be the even extension of the ion potential energy at coordinate ζ, as pictured in Fig. 2. $\psi(\zeta) = e_0\Psi/k_BT$ is the corresponding dimensionless quantity.

First construct a sequence of random walks leading to the Smoluchowski equation for the ion in the potential energy well. The random walk involves steps between n sites spaced uniformly across the even extension of the boundary layer at $\zeta_i = \zeta_0(-1 + 2i/n)$, $1 \le i \le n$. A walker steps from site i to site $i + 1$ with probability δ_i and from site i to site $i - 1$ with probability $\hat{\delta}_i$. These transition probabilities are defined by

$$\delta_i = \Delta t D \mathcal{L}^{-2}(n^2 - n\mathcal{L}\psi_i'/2) \tag{57}$$

$$\hat{\delta}_i = \Delta t D \mathcal{L}^{-2}(n^2 + n\mathcal{L}\psi_i'/2), \tag{58}$$

where $\mathcal{L} = 2\zeta_0$ is the length of the extended potential profile, Δt is the time interval between steps, and $\psi'_i = \psi'(\zeta_i)$, with the prime denoting a derivative with respect to ζ. So that the sum of the transition probabilities never exceeds 1, it is necessary to also scale Δt with n, as shown by Eq. 14. Let $P_i(t)$ be the probability that a walker occupies site i at time t. The change in this probability over one time step is

$$\begin{aligned} &P_i(t + \Delta t) - P_i(t) \\ &\quad = P_{i+1}(t)\hat{\delta}_{i+1} + P_{i-1}(t)\delta_{i-1} - P_i(t)(\delta_i + \hat{\delta}_i). \end{aligned} \tag{59}$$

Suppose site i is associated with a boundary layer slice of thickness $\mathcal{L}/n$ and a surface of area A. If $C_i(t)$ is the concentration of random walker associated with site i, then

$$P_i(t) = C_i(t)A\mathcal{L}/n, \tag{60}$$

where $C_i(t) = C(\zeta_i, t)$. Substituting Eqs. 57, 58, and 60 into Eq. 59 and dividing by $\Delta t A\mathcal{L}/n$, we obtain

$$\begin{aligned} &[C_i(t + \Delta t) - C_i(t)]/\Delta t \\ &\quad = D\mathcal{L}^{-2}n^2[C_{i+1}(t) + C_{i-1}(t) - 2C_i(t)] \\ &\quad + D\mathcal{L}^{-1}(n/2)[\psi'_{i+1}C_{i+1} - \psi'_{i-1}C_{i-1}], \end{aligned} \tag{61}$$

where we recognize that the first term on the right-hand side is proportional to a second difference, and the second term is proportional to a symmetrical first difference. Let $n \to \infty$ and $i \to \infty$, scaling i so that $\zeta_i \to \zeta$, to obtain the Smoluchowski equation,

$$\frac{\partial C}{\partial t} = D\frac{\partial^2 C}{\partial \zeta^2} + D\frac{\partial}{\partial \zeta}(\psi' C). \tag{62}$$

This equation describes diffusion biased by the interaction ψ with the membrane surface. Equation 1 may be obtained in a similar way, generalizing to three dimensions.

We now consider the problem of calculating the mean time to escape the extended boundary layer, that is, to reach the boundary $\zeta = -\zeta_0$ or $\zeta = \zeta_0$ in the limit $n \to \infty$. Let $\hat{T}_i$ be the mean time before a diffuser, starting at site i, reaches one of the end points $\zeta_1 = \zeta_0(-1 + 2/n)$ or $\zeta_n = \zeta_0$. Suppose this process starts at initial time t_0. For some fixed lattice site i, $2 \le i \le n - 1$, we have

$$\begin{aligned} P_i(t_0) &= 1, \\ P_j(t_0) &= 0, \end{aligned} \tag{63}$$

for $i \ne j$. Let $\tilde{T}(t)$ be the mean time before the diffuser reaches an end point, averaged over the distribution of lattice site probabilities at time t. Then $\tilde{T}/(t_0) = \hat{T}_i$. After one time step,

$$\tilde{T}(t_0 + \Delta t) = \hat{T}_i - \Delta t \tag{64}$$

and

$$\begin{aligned} P_i(t_0 + \Delta t) &= 1 - \delta_i - \hat{\delta}_i, \\ P_{i-1}(t_0 + \Delta t) &= \hat{\delta}_i, \\ P_{i+1}(t_0 + \Delta t) &= \delta_i. \end{aligned} \tag{65}$$

The mean time before the diffuser escapes is now a weighted average:

$$\tilde{T}(t_0 + \Delta t) = P_i(t_0 + \Delta t)\hat{T}_i + P_{i+1}(t_0 + \Delta t)\hat{T}_{i+1} + P_{i-1}(t_0 + \Delta t)\hat{T}_{i-1}. \quad (66)$$

Substitute Eqs. 57, 58, 64, and 65 into Eq. 66, subtract $\hat{T}_i$ from both sides, and divide by Δt to obtain

$$-1 = D\mathcal{L}^{-2}n^2(\hat{T}_{i+1} + \hat{T}_{i-1} - 2\hat{T}_i) - D\psi_i'\mathcal{L}^{-1}(n/2)(\hat{T}_{i+1} - \hat{T}_{i-1}). \quad (67)$$

The limit $n \to \infty$, $i \to \infty$, such that $i/n \to \zeta$, gives

$$-1 = D\left(\frac{\partial^2\hat{T}}{\partial\zeta^2} - \psi'\frac{\partial\hat{T}}{\partial\zeta}\right), \quad (68)$$

where $\hat{T}_i = \hat{T}(\zeta_i)$. The appropriate boundary conditions are clearly $\hat{T}(-\zeta_0) = \hat{T}(\zeta_0) = 0$.

This equation can be solved by the method of variation of parameters. The general solution has the form

$$D\hat{T}(\zeta) = -\int_{-\zeta_0}^{\zeta}[s(\zeta) - s(\zeta')]e^{-\psi(\zeta')}d\zeta' + K_1 s(\zeta) + K_2, \quad (69)$$

where

$$s(\zeta) = \int_{-\zeta_0}^{\zeta} e^{\psi(\zeta')}d\zeta'. \quad (70)$$

Satisfaction of the boundary conditions and a rearrangement of the integral results in

$$D\hat{T}(\zeta) = \left(1 - \frac{s(\zeta)}{s(\zeta_0)}\right)\int_{-\zeta_0}^{\zeta} s(\zeta')e^{-\psi(\zeta')}d\zeta' + \frac{s(\zeta)}{s(\zeta_0)}\int_{\zeta}^{\zeta_0}[s(\zeta_0) - s(\zeta')]e^{-\psi(\zeta')}d\zeta'. \quad (71)$$

This is the formula for the mean first passage time. It is both symmetrical, $\hat{T}(\zeta) = \hat{T}(-\zeta)$, and differentiable. It follows that $\hat{T}'(0) = 0$. Therefore, in the physical region $\zeta \geq 0$, our solution is equivalent to the solution of Eq. 68 with boundary conditions $\hat{T}'(0) = \hat{T}(\zeta_0) = 0$. The solution in the extended interval has the merit of making the assumed behavior of ion trajectories at the membrane surface completely clear.

Numerical integration

Evaluating Eq. 71 for the Gouy-Chapman potential sketched in Fig. 5 is an exercise in numerical integration. The formula was evaluated using a dimensionless independent variable η defined by $\zeta = \zeta_0(2\eta - 1)$, with $0 \leq \eta \leq 1$. We then took a multistep approach. The function $s(\zeta)$ was evaluated by the NIntegrate function of Mathematica 3.0 (Wolfram, 1996) at 21 uniformly spaced values of η (0, 0.05, etc.). The resultant ordered pairs were used as nodes to define a spline interpolant, which in turn was used provide values of $s(\zeta')$ in the integrand of Eq. 71. The NIntegrate function was used again to evaluate $\hat{T}(\zeta)$ at the same 21 values of η to construct a second spline interpolant for use in the integrand of Eq. 27. As a numerical check, the number of nodes used in both stages of interpolation was reduced to 11, without a significant change in the result.

We thank Kevin Cooper, Peter Jordan, Valipuram Manoranjan, and Roderick MacKinnon for helpful discussions.

This work was supported by grants MCB 94-04430 and 96-30475 from the National Science Foundation.

REFERENCES

Adams, G., and M. Delbrück. 1968. Reduction of dimensionality in biological diffusion processes. *In* Structural Chemistry and Molecular Biology. A. Rich and N. Davidson, editors. W. H. Freeman and Company, San Francisco. 198–215.

Aguilella, V., T. K. Rostovtseva, I. Vodyanoy, S. M. Bezrukov, and V. A. Parsegian. 1997. Gramicidin A channel as a sensor: a membrane lipid titration. *Biophys. J.* 72:A395.

Apell, H.-J., E. Bamberg, and P. Laüger. 1979. Effects of surface charge on the conductance of the gramicidin channel. *Biochim. Biophys. Acta.* 552:369–378.

Bell, J. E., and C. Miller. 1984. Effects of phospholipid surface charge on ion conduction in the K^+ channel of sarcoplasmic reticulum. *Biophys. J.* 45:279–287.

Berg, H. C., and E. M. Purcell. 1977. Physics of chemoreception. *Biophys. J.* 20:193–219.

Chiu, S.-W., and E. Jakobsson. 1989. Stochastic theory of single occupied channels. II. Effects of access resistance and potential gradients extending into the bath. *Biophys. J.* 55:147–157.

Eisenberg, M., T. Gresalfi, T. Riccio, and S. McLaughlin. 1979. Adsorption of monovalent cations to bilayer membranes containing negative phospholipids. *Biochemistry.* 18:5213–5223.

Hall, J. E. 1975. Access resistance of a small circular pore. *J. Gen. Physiol.* 66:531–532.

Hille, B. 1992. Ionic Channels of Excitable Membranes, 2nd Ed. Sinauer Associates, Sunderland, MA.

Jackson, J. D. 1975. Classical Electrodynamics, 2nd Ed. John Wiley and Sons, New York.

Karlin, S., and H. M. Taylor. 1981. A Second Course in Stochastic Processes. Academic Press, New York.

Läuger, P. 1976. Diffusion-limited ion flow through pores. *Biochim. Biophys. Acta.* 455:493–509.

Levitt, D. G. 1986. Interpretation of biological ion channel flux data: reaction rate versus continuum theory. *Annu. Rev. Biophys. Biophys. Chem.* 15:29–57.

Lifson, S. 1962. On the self-diffusion of ions in a polyelectrolyte solution. *J. Chem. Phys.* 36:2410–2414.

McGill, P., and M. F. Schumaker. 1996. Boundary conditions for single-ion diffusion. *Biophys. J.* 71:1723–1742.

McLaughlin, S. 1977. Electrostatic potentials at membrane-solution interfaces. *Curr. Top. Membr. Transp.* 9:71–144.

Nelson, A. P., and D. McQuarrie. 1975. The effect of discrete charges on the electrical properties of a membrane. I. *J. Theor. Biol.* 55:13–27.

Risken, H. 1989. The Fokker-Planck Equation. Springer Verlag, New York.

Smythe, W. R. 1968. Static and Dynamic Electricity, 3rd Ed. McGraw-Hill, New York.

Wolfram, S. 1996. The Mathematica Book, 3rd Ed. Wolfram Media and Cambridge University Press, New York.